IOP Conf. Series: Materials Science and Engineering **174** (2017) 012030 doi:10.1088/1757-899X/174/1/012030

Two-way coupled Reynolds, Rayleigh-Plesset-Scriven and energy equations for fully transient cavitation and heat transfer modeling

M Braun, K Pierson and T Snyder

Department of Mechanical Engineering, The University of Akron, Akron, OH, USA

E-mail: mjbraun@uakron.edu

Abstract. The Rayleigh-Plesset-Scriven (RPS) equation representing the source of void production is coupled with the Reynolds (RE) and energy equations in a fully transient solution with feedback between these equations. Temperature effects are accounted for by using an energy equation integrated across the bearing film. Dynamic enlargement of the surface of each of the discrete bubbles forming the pseudo-cavitation zone is accounted for by introducing the surface dilatational viscosity term in the RPS equation; this represents a continuation of previous work by Snyder et al [1] that established parametrically the significance of the surface dilatational viscosity (k^s=3.75*10^{-3} N.s/m) both in the development of the cavitation bubble and the formation and sustenance of the subcavitation tensile forces. The study presents the interlaced effects of residual fluid internal energy, eccentricity, angular velocity and heat transfer coefficient on the pressure and pseudo-cavitation development.

Nomenclature

c	Specific heat of oil
h, h_0, h_h	Heat transfer coefficient
H	Thickness of thin film
k	Thermal conductivity of oil
P, P_B, P_G, P_v	Pressure, total pressure inside the bubble, pressure of the gas, vapor pressure
P_R, P_∞	Pressure directly outside of bubble wall, and pressure in the liquid far from the bubble
Q_{gen}	Heat generation due to viscous dissipation
Q_{res}	Q_{gen} less the amount of heat lost from convection to bearing components
R_B	Cavitating bubble radius
t	Time
T	Temperature of mixture
$\bar{u}, \bar{w}$	Average velocity of mixture in $x-$ and $y-$ direction respectively
V_{cell}	Volume of computational cell
x, y	Spatial coordinates: along the unwrapped surface, axial
α	Void fraction
γ	Surface tension of bubble
ε	Bearing eccentricity ratio

κ, κ^s	Bulk dilatational viscosity, Surface Dilatational Viscosity
μ, μ_l, μ_B	Dynamic viscosity of mixture, liquid (oil) and bubble.
ν_L	Kinematic viscosity of liquid (oil)
ρ, ρ_l, ρ_B	Density of mixture, liquid and gas bubble respectively

1. Introduction

There is a plethora of literature treating pseudo-, vaporous and gaseous cavitation, a difficult and complex problem that requires an interdisciplinary approach to solution. There has been steady progress in the understanding of this problem, starting with the initial treatise of Osborne Reynolds [2] in 1886 and Sommerfeld [3] in 1904, to today's state of the art which offers a multi physics model and numerical implementation (Someya [4], Natsumeda and Someya [5], Gehanin et al. [6, 7], Snyder et al. [1]). Early, nonconservative cavitation models were followed by mass conserving models, which assumed striated flows formed out of gas fingers interspersed with liquid regions extending across the clearance. In the last 75 years, numerous innovative analytical and numerical solutions, as well as seminal experimental findings were offered. In this context, the reader is further referred to the review publications of Dowson et al. [8], Brewe et al. [9], Braun and Hannon [10] and Snyder et al [1]. Zuber and Dougherty [11] in 1982 proposed a Reynolds equation (RE) that introduced a homogeneous two-phase lubricating film mixture as the working fluid. Natsumeda and Someya [5] in 1987 also used the concept of a homogeneous two-phase flow RE coupled with the Rayleigh-Plesset-Scriven (RPS) equation as the void generation source for the homogeneous two-phase film. Notably, the RPS equation differs from the classical Rayleigh-Plesset equation through the inclusion of viscous surface dilatation effects ($\frac{4\kappa^s}{\rho_l R_B^2}\dot{R}_B$). These effects have proven to have a major role in both the physical sustenance of the subcavity tensile forces (measured to be as high as 1.2 MPa), and the numerical stability of the RPS equation. The importance for the stability of the numerical computations has been clearly recognized by both work of Gehannin et al. [7, 12] and Natsumeda [5] and Someya [4]. The RPS equation solves for the bubble radius growth $R(t)$, independent of inertia effects, thus providing the mechanism for void fraction, α, generation and its change with respect to time, implicitly contributing to the calculation of the two-phase homogeneous ρ and μ used in the RE.

2. Scope of work

By adding the energy equation, the present work extends the work of Snyder et al. [1] regarding the development of pseudo-cavitation (no mass transfer by diffusion, or evaporation). In the present development, the collection of kernel bubbles grow both due to depressurization and temperature change, as the RE and RPS equations are coupled in a feedback loop with a two-dimensional energy equation lumped across the film thickness. Thus, the void fraction α, the liquid and bubble densities ($\rho_L$and ρ_B), as well as their viscosities ($\mu_L$and μ_B), vary both in the circumferential and axial directions (x, z) with both pressure and temperature. The two dimensional energy equation (x, z) incorporates the effects of convection-conduction heat transfer at the fluid boundaries with the shaft and bushing. The calculation of the void fraction, α, as a function of (x, z, t, and T) at every grid point allows transient calculation of local homogeneous two-phase film density and viscosity in conjunction with the transient form of the RPS, RE and energy equations. The results account for cavitation, pressure, temperature and void fraction development when the fluid heat transfer coefficient, h_0=h_h=h, is varied parametrically, while eccentricity, angular velocity, and surface dilatational viscosity are kept constant.

3. On the surface dilatational viscosity

In a fluid at rest, the hydrostatic stress ($-\bar{P}$) is the same as the thermodynamic pressure. However, for a fluid in motion, the total normal stress, σ_{ii}, deviates from the thermodynamic pressure. One can write a relationship between the symmetric components of the deviatoric stress tensor and the thermodynamic pressure and relate to the average pressure, $\bar{P}$, equation 1

$$-\bar{P} = \bar{\sigma} = \frac{\sigma_{ii}}{3} = \left(\frac{2\mu}{3} + \lambda\right)\frac{\partial u_i}{\partial x_i} - p \tag{1}$$

where $(\frac{2\mu}{3} + \lambda) = \kappa$ is defined as bulk (dilatational) viscosity. While μ represents the dynamic shear viscosity of the fluid, the physical meaning of λ is associated with viscous dissipation as it relates to volumetric change, Schlichting [13]. In three-dimensional fluids, generally Stokes hypothesis is applied, wherein the thermodynamic and mechanical pressures are taken to be equal, i.e. $\lambda = -2\mu/3$ and $\kappa = 0$. However, unlike κ, its two-dimensional analog κ^s (surface dilatational viscosity) does not vanish when it is present in two-phase fluids and can greatly affect the dynamic interfacial balance of forces for a bubble growing through pseudo-cavitation, evaporation or gas diffusion. A stress balance calculated at the bubble's wall, yields

$$\Delta\sigma_{fluid-bubble} = \frac{2\gamma}{R_B} + \frac{4\kappa^s}{R_B^2}\dot{R}_B \tag{2}$$

where, in an active expanding/contracting environment the dynamic tension at the interface exceeds the equilibrium tension, $\frac{2\gamma}{R_B}$, by the quantity $\frac{4\kappa^s}{R_B^2}\dot{R}_B$. The latter through its derivative $\dot{R}_B$, always exerts an action opposing the motion of the bubble wall resulting in an interfacial stress jump that causes the deviation from the static case.

4. Bubble dynamics

The Rayleigh [14] bubble dynamics equation describes the growth and collapse of an isolated, spherical bubble driven only by a varying external pressure field. The inclusion of interfacial rheological stresses is necessary (Scriven [15]) when the ratio of the interfacial area-to-volume is large, which is the case of the journal bearing or squeeze film dampers. If viscous effects within the gas bubble are neglected and the liquid surrounding the bubble is considered to be Newtonian and incompressible (κ = 0, Stokes hypothesis), the dynamic surface stress balance yields to a modified pressures in the liquid adjacent to the bubble wall, P_R, of the form (Snyder et al. [1])

$$P_R = P_B - 4\frac{\mu_L\dot{R}}{R} - \frac{2\gamma}{R} - \frac{4\kappa^s\dot{R}}{R^2} \tag{3}$$

Further, replacing P_R in Rayleigh's equation with its expression given by equation 3 results in a bubble dynamics equation which accounts for all of the interfacial properties

$$(R\ddot{R} + \frac{3}{2}\dot{R}^2) + 4\frac{\nu_L\dot{R}}{R} + \frac{2\gamma}{\rho_L R} + \frac{4\kappa^s\dot{R}}{\rho_L R^2} = \frac{P_B - P_\infty}{\rho_L} \overset{Daltonlaw}{=} \frac{P_G + P_v - P_\infty}{\rho_L} \tag{4}$$

In equation 4, the bubble contents are considered to be a mixture of both vapor and non-condensible gas(es) where by virtue of Dalton law of partial pressures one can write that $P_B = P_G + P_v$. For the P_G variation one may consider a polytropic transformation, Snyder et al. [1], $(P_G = \frac{P_{G0}}{\rho_L}\left(\frac{R_0}{R}\right)^{3n})$ or the Combined Gas Law (CGL) $(P_G = \frac{P_{G0}}{\rho_L}\left(\frac{R_0}{R}\right)^3\frac{T_G}{T_{G0}})$. In the latter case the variation of temperatures require that the energy equation be coupled with the RE and the RPS equations.

5. The physical model

The proposed pseudo-cavitation model involves the feedback coupling between the RE, RPS and the energy equations. This occurs through the exchange of values of the film pressure (RE) and variable bulk properties $\mu = \mu[\alpha\,(x,z,T)]$ and $\rho = \rho[\alpha(x,z,T)]$ of the two phase mixture, and adjustment of the void fraction by means of the combination of equation 4 with the Combined Gas Law and energy equation. The local film pressure P is computed by the RE, and by entering the pressure driving term into the RPS equation, these two equations are coupled. The bubble is assumed to contain a single non

-condensable gas kernel undergoing a transformation consistent with equation 4 and the CGL, but neglecting the inertia terms.

$$4\frac{\nu_L\dot{R}}{R}+\frac{2\gamma}{\rho_L R}+\frac{4\kappa^s\dot{R}}{\rho_L R^2}=\frac{P_{G0}}{\rho_L}\left(\frac{R_0}{R}\right)^3\frac{T_G}{T_{G0}}-\frac{P}{\rho_L} \tag{5}$$

The change in bubble radii is used to compute the local cell void fraction through the ratio of a spherical bubble volume to the local computational cell volume as

$$\alpha=\frac{4/3\pi R^3}{V_{cell}} \tag{6}$$

The particular shape of the bubble is not considered to be of consequence insomuch as limiting the validity of the bubble dynamics equation, or its usefulness for the present application. With no simple or practical alternative approach for non-spherical bubble dynamics, the spherical bubble symmetry is assumed to be maintained.

If the bulk density and dynamic viscosity of the fluid film are considered to be continuous functions of a homogeneous two-phase fluid similar to the one used by Zuber and Dougherty [11], they may be expressed through the component properties and the void fraction as

$$\rho=\alpha\rho_G+(1-\alpha)\rho_L;\quad \mu=\alpha\mu_G+(1-\alpha)\mu_L \tag{7a,b}$$

In equations 7a and 7b, ρ_L and μ_L are functions of the temperature [16] yielded by the energy equation presented below, equation 9. In regard to the fluid film, the laminar, transient, variable property form of the Reynolds equation can be written as

$$\frac{\partial}{\partial x}\left(\frac{\rho(\alpha)h^3}{12\mu(\alpha)}\frac{\partial P_R}{\partial x}\right)+\frac{\partial}{\partial y}\left(\frac{\rho(\alpha)h^3}{12\mu(\alpha)}\frac{\partial P_R}{\partial y}\right)=\frac{\partial}{\partial x}\left(\frac{\rho(\alpha)hU}{2}\right)+\frac{\partial(\rho(\alpha)h)}{\partial t} \tag{8}$$

The energy equation in its transient form, lumped across the fluid film takes the form

$$\frac{\partial(cT)}{\partial t}+\bar{u}\frac{\partial(cT)}{\partial x}+\bar{w}\frac{\partial(cT)}{\partial y}=\frac{1}{\rho}\frac{\partial}{\partial y}\left(k\frac{\partial T}{\partial y}\right)-\frac{1}{\rho H}\left[h_h(T-T_{\infty 1})+h_0(T-T_{\infty 2})-Q_{gen}\right] \tag{9}$$

The last three terms of the RHS of equation 9 represent the heat lost by convection to the shaft and bushing (where $h_0=h_h=h$), and the heat generated due to frictional dissipation, respectively. The field equations written in Cartesian coordinates are applied to an unwrapped bearing fluid film, figure 1.

6. Results and discussion of the parametric variation the heat transfer coefficients.

All results presented herein are obtained for a journal bearing with an eccentricity of $\varepsilon=0.8$ running at an angular velocity of 5 krpm. Figure 2 presents a composite of 2-D line graphs at the axial center line for pressure, void, mixture viscosity, residual heat carried by the fluid and temperature, as the convective heat transfer coefficient (HTC) varies from 10 to isothermal conditions (HTC>>1000 W/m^2°C). This combined presentation is intended to facilitate the understanding of the interaction between these parameters. In figure 2a, the pressure decreases, as the HTC decreases from 1000 to 10 W/m^2°C. It is noteworthy that for the same trend of HTC (decrease by two orders of magnitude), the temperature raises by a factor of 2, figure 2d, while viscosity decreases by a factor of approximately 4 in the region confined between 90 and 200, figure 2e. The decrease in viscosity at the same temperature is driven mainly by the change in the void fraction, while its decrease at the different HTCs different is driven by the increase in temperature as HTC goes down. A comparative look at figures 2b and 2e, shows the most dramatic decrease in the mixture viscosity in the regions between 90° and 200° even though, between the same angle confines, the void fraction is essentially zero, figure 2b. This indicates that μ_L is the dominant quantity in the mixture viscosity with void playing almost no role. The driver of the entire development described above is Q_{res}, representing the amount

of residual enthalpy left in the fluid when parts of the Q_{gen} are lost due to convection to the shaft and bushing. Most generally, as HTC decreases, less heat is lost, resulting in highest temperatures at $h = 10\ \mathrm{W/m^2{}^\circ C}$. As the HTCs are increased by a factor of 10 and 100 respectively, the temperatures trend lower (by almost a factor of 2). This is justified by an increased heat loss as the increase in the HTC outweighs the decrease in temperatures.

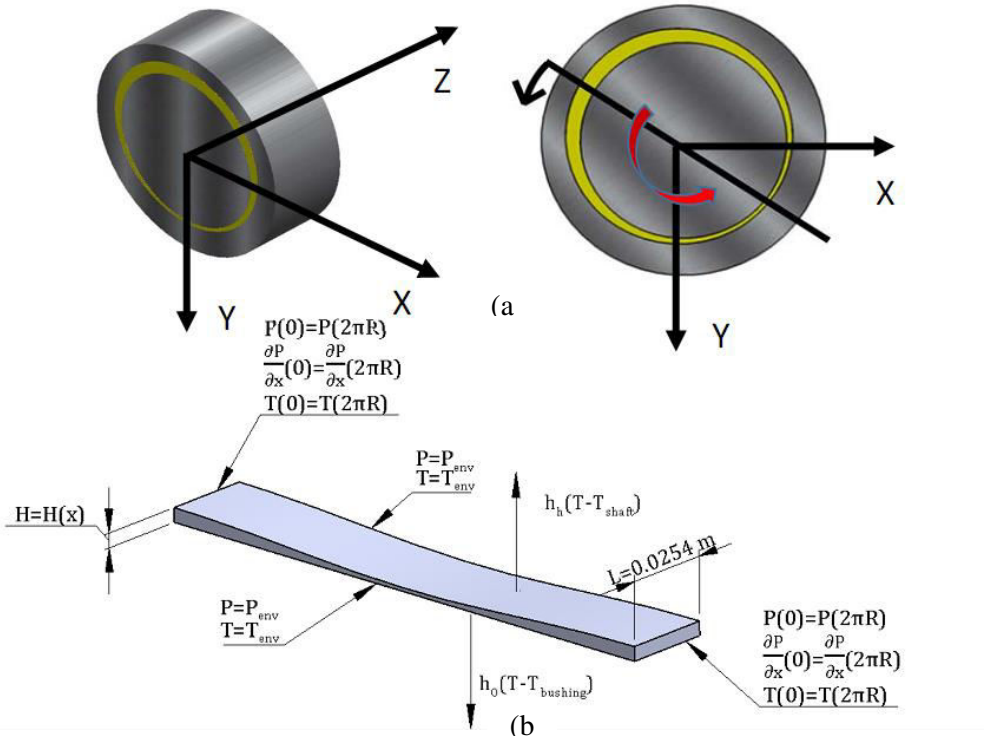

Figure 1. Geometry of the unwrapped bearing: (a) lateral and frontal view; (b) unwrapped film with Reynolds and energy equations boundary conditions. $T_{env} = T_{shaft} = T_{bushing} = 80°C$; $P_{env} = 1$ atm; $h_h = h_0 = h$.

Thus, counter-intuitively more heat is lost at lower temperatures than at the higher ones. The HTC, and not the temperature magnitude is responsible for this phenomenon. Figure 3 presents the temperature development in the fluid over the entire surface of the fluid in the unwrapped fluid film when $\varepsilon = 0.8$ and the angular velocity is 5 krpm. For direct comparison purposes all three figures are plotted at the same scale. Figure 3a presents the temperature variation when HTC is $10\mathrm{W/m^2\ ^oC}$. Highest temperatures are observed here since this case corresponds to the lowest HTC. It appears the highest values occur, as expected, at the center line and continue almost unabated for the entire circumference (see also figure 2), though the width of this band is rather narrow. The lower temperatures that prevail on the outer axial regions are due to the boundary conditions which provide for fluid at 80°C temperature entering axially the bearing. The effects of these lower temperatures penetrate gradually towards the center where they meet a high temperature band. The same effect is visible, though less pronounced in figure 3b. The higher pressure achieved in the case of $h = 100\,\frac{\mathrm{W}}{\mathrm{m^2}}{}^\circ C$, allows more penetration of the temperatures towards the axial ends of the bearing creating larger bands of higher temperatures throughout the bearing. Figure 3c presents the case for $h = 1000\ \mathrm{W/m^2{}^\circ C}$. Even though this case is associated with the lowest temperature developing inside the bearing, the heat generation is the highest (figure 2c) due to higher viscosity (figure 2e).

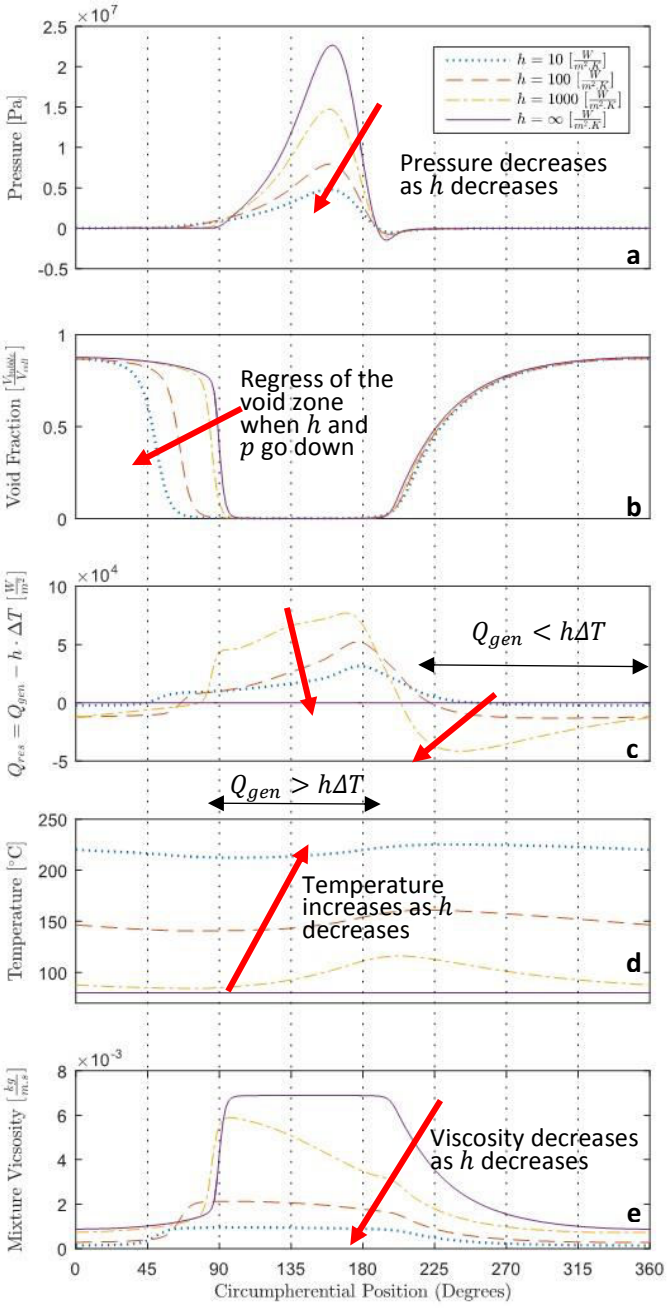

Figure 2. Study of the parametric effects of the heat transfer coefficient on the journal bearing behavior, $\varepsilon = 0.8$, angular velocity = 5 krpm. a) Pressure; b) void, α; c) fluid residual heat Q_{res}; d) temperatures; e) mixture dynamic viscosity.

Figure 4 presents the pressure development when the heat transfer coefficient is varied. The discussion of the centerline pressures behavior has been offered in figure 2. This figure presents the 2-D contour plots covering the entire surface of the bearing and rendering the two dimensional formation both of the cavity zone and the subcavity tensile region. Figures 4a-4d present the evolution

of the overall pressures as the heat transfer coefficient is increased from 10 to 1000 W/m^2°C. For comparison purposes the isothermal case ($h \rightarrow \infty$) is presented in figure 4d.

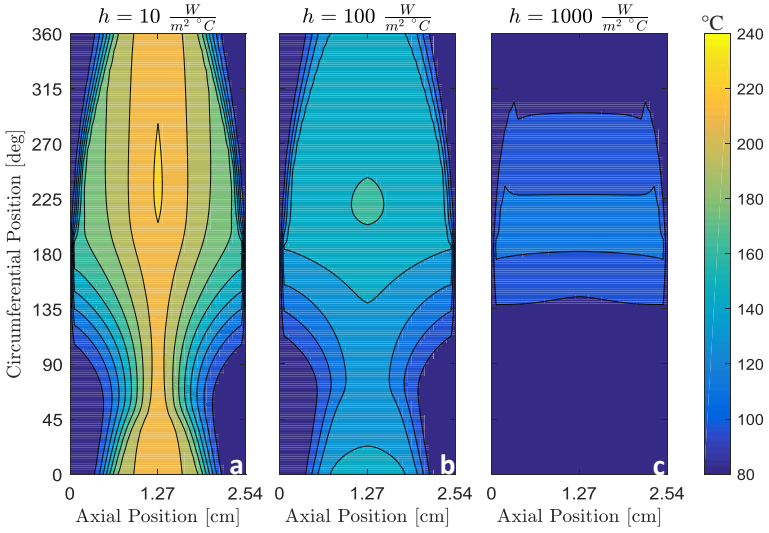

Figure 3. Temperature contour plots for bearing temperature for parametric variation of the heat transfer coefficient when $\varepsilon = 0.8$, angular velocity=5 krpm.

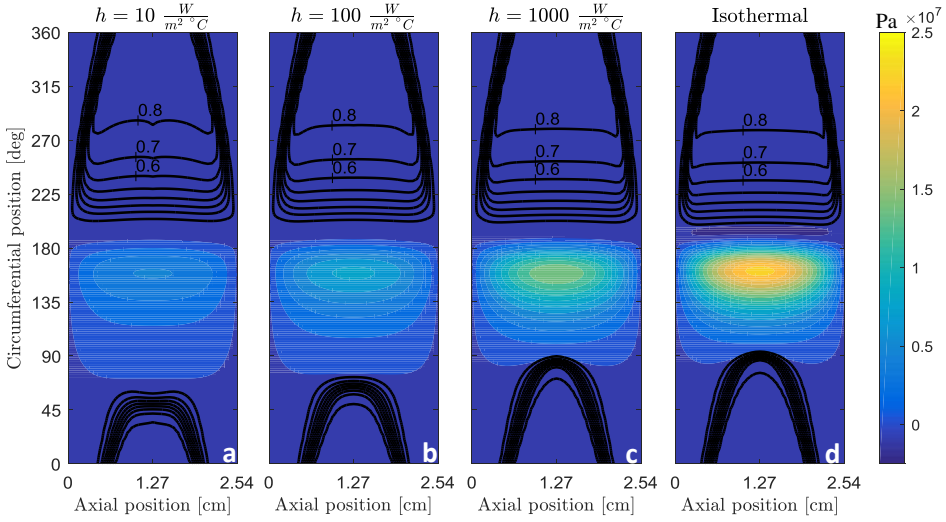

Figure 4. Pressure contour plots for bearing pressure and void fraction for parametric variation of the heat transfer coefficient when ε=0.8, angular velocity=5 krpm.

One can see clearly the evolution of the pressure contour curves from the lowest pressures $at\ h = 10\ W/m^2$°C, with practically no subcavity pressure present to the highest pressure for the isothermal case and the largest subcavity zone. The size of the subcavity is related to both surface dilatational viscosity [1] and the overall temperature levels. The figure also presents, in 2-D, the extent and growth of the cavity zone from its lowest expanse associated with the lowest pressure levels, to its highest, associated with the highest pressures.

7. Conclusions

The present study endeavors to detail the temperature effects on pressure, void, mixture viscosity and subcavity development when an axial-circumferential energy equation is fully coupled with a variable

properties Reynolds, Rayleigh-Plesset-Scriven equations as well as the temperature dependent μ and ρ. It has been shown that the void development is largely dependent on the pressure variations while also being influenced by the temperature levels (figure 2b). Viscosity decreases significantly with temperature (figure 2c), while the latter is basically dependent on the Q_{res} left in the fluid following heat losses from the film to the shaft and bushing. Counterintuitively, both the highest heat generation and heat losses happen for the lowest temperature, (figures 2c and 2d), resulting from the joint effects of temperature decrease with increasing HTC and decrease of mixture viscosity with temperature.

References

[1] Snyder T, Braun M and Pierson K 2016 Two-way coupled Reynolds and Rayleigh–Plesset equations for a fully transient, multiphysics cavitation model with pseudo-cavitation *Tribol. Int.* **93** 429-445
[2] Reynolds O 1886 On the theory of lubrication and its application to Mr. Beauchamp Tower's experiments including an experimental determination of the viscosity of olive oil *Phil. Trans. R. Soc. Lond.* **177** 157-234
[3] Sommerfeld A 1904 Zur hydrodynamische Theorie der Schmiermittelreibung *Zeit. Math. Phys.* **50** 97-155
[4] Someya T 2003 On the development of negative pressure in oil film and the characteristics of journal bearing *Meccanica* **38** 643-658
[5] Natsumeda S and Someya T 1987 negative pressures in statically and dynamically loaded 6journal bearings Paper III (ii) *Proc. of the 13th Leeds-Lyon Symp. on Tribology (Tribology Series* **11***)* ed D. Dowson et al. (Amsterdam: Elsevier) 65-72
[6] Gehannin J, Arghir M and Bonneau O 2015 A volume of fluid method for air ingestion in squeeze film dampers *Tribol T* **59** 208-218
[7] Gehannin J, Arghir M and Bonneau O 2010 Complete squeeze film damper analysis based on the bulk flow equations *Tribol T* **53** 84-95
[8] Dowson D, Godet M and Taylor CM 1974 Cavitation and related phenomena in lubrication *Proc. of the 1st Leeds-Lyon Symp. on Tribology* (London; New York: Mechanical Engineering Publications Ltd) 1-238
[9] Brewe D E 1986 Theoretical modeling of the vapor cavitation in dynamically loaded journal bearings *J. Tribology* **108** (4) 628-638
[10] Braun M and Hannon W 2010 Cavitation formation and modelling for fluid film bearings: a review *P. I. Mech. Eng. J-J Eng.* **224** (9) 839-86
[11] Zuber N and Dougherty D 1982 The field equations for two-phase Reynolds film flow with change of phase *ASLE Trans.* **25** (1) 108-116
[12] Gehannin J. Arghir M and Bonneau O 2009 Evaluation of the Rayleigh-Plesset equation based cavitation models for squeeze film dampers *J. Tribology* **131** (2) 15-25
[13] Schlichting H 1979 *Boundary layer theory* (7th ed.) (New York: McGraw Hill) 60-63
[14] Rayleigh L 1917 On the pressure developed in a liquid during the collapse of a spherical cavity *The London, Edinburgh, and Dublin Philosophical Magazine and Journal of Science* **34** (200) 94-98
[15] Scriven L 1960 Dyamics of a fluid interface. Equation of motion for Newtonian surface fluids *Chem. Eng. Sci.* **12** (2) 99-108
[16] Bruce RW 2012 *Handbook of lubrication and tribology, Volume II: Theory and design, Second Edition* (Boca Raton: CRC Press) 458-459